

DETECTING OBJECTS UNDER SHADOWS BY FUSION OF HYPERSPECTRAL AND LIDAR DATA: A PHYSICAL MODEL APPROACH

Qiang Zhang, V. Paúl Pauca, Robert J. Plemmons*

Wake Forest University
Departments of Mathematics and Computer Science

D. Dejan Nikic*

The Boeing Company, Inc.

ABSTRACT

Due to lack of direct illumination, objects under shadows often reflect significantly fewer numbers of photons into a remote hyperspectral imaging (HSI) sensor, leading to low radiance levels near to or below noise. Attempts to perform object classification based on these observed radiances often produce poor results, grouping pixels under shaded areas as being a part of the same class. By fusing LiDAR and HSI data through a physical model, we develop a simple and efficient illumination correction method to remove the direct illumination component of the observed HSI radiance data. This correction then enables accurate object classification, regardless of whether or not spectral signatures are exposed directly to sunlight. In addition, methods for estimating the areas under shadows and geometric parameters such as direct illumination factor and sky-view factor from LiDAR data are presented.

Index Terms— Hyperspectral and LiDAR data fusion, object detection under shadow, radiance model, sky-view factor.

1. INTRODUCTION

Hyperspectral imaging (HSI) data is important in many fields such as environmental remote sensing, monitoring chemical/oil spills, and military target discrimination [1]. It is also of high interest in security and defense applications where objects may need to be detected, classified, and identified. Detecting or classifying an object under shadows using HSI data can be particularly challenging [2]. Figure 1 shows the radiance spectral signatures of two pixels of the same material obtained from the same dataset. Specifically, one pixel was extracted from the shaded part of a slanted roof and the other from the roof side directly exposed to the sun. As can be observed, the radiance of the pixel with direct sun exposure is significantly higher than that of the pixel under shadow. The apparent and significant differences in magnitude and shape of the spectral radiances can make it hard to classify these

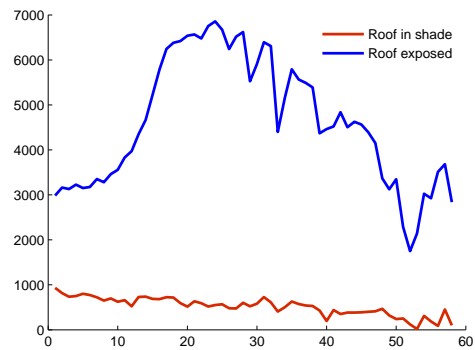


Fig. 1. Comparison of the radiance spectral signatures of two pixels on two slanted roofs facing to and away from sun.

pixels as belonging to the same material by their radiance vectors only.

LiDAR (Light Detection And Ranging, also LADAR) is an optical remote sensing technology that can measure the distance to a target by illuminating the target with pulses from a laser [?]. This range data, once combined with HSI data, can provide a more comprehensive picture of objects on the ground. For example, LiDAR data alone could not be used to differentiate grassy areas from roads on the same flat surface, while HSI spectral signatures can. On the other hand, HSI spectral signatures could not be used to differentiate roofs from roads if both are made with the same asphalt, while LiDAR data can. The fusion of HSI data with LiDAR data is promising technique for enabling the extraction of a variety of information from the data ensemble and as such is a current topic in remote sensing, see e.g., [3, 4].

The fusion of HSI and LiDAR has been suggested in the literature for detecting objects under shadows. Shimoni et al [5] employ a score-level fusion approach for detecting stationary vehicles under shadows, where detection scores from both HSI and LiDAR data are derived separately and combined for joint detection using a simple sum rule. In a type of model-level fusion approach, Ientilucci [6] combines HSI and LiDAR data through a forward radiance model that in-

*Research sponsored in part by the U.S. National Geospatial-Intelligence Agency under Contract HM1582-10-C-0011, public release number PA Case 13-192.

cludes direct illumination and diffused skylight components of radiance. The model allows removal of the direct illumination component and with this correction, similar objects can show highly correlated radiances across bands. Here, we modify Ientilucci’s approach and eliminate the need for specialized software such as MODTRAN [?] in the algorithmic solution. In addition, we provide simplified methods for calculating geometric parameters such as sky-view factors from LiDAR data, without the need for additional software packages.

The remainder of the paper is organized as follows. In Section 2, we introduce a simplified radiance model combining HSI and LiDAR data and present a de-shadowing approach. In Section 3, we present results of this approach on co-registered HSI and LiDAR datasets. Conclusions and final remarks are provided in Section 4.

2. MODEL

2.1. Radiance Model

According to [7], there are essentially four types of photons reaching an airborne sensor from a target when the source of light is the sun: photons directly emitted by the sun and reflected by the target; photons scattered by aerosols and then reflected by the target, also called diffused skylight; photons bouncing from surrounding objects and reflected by the target; and photons scattered by aerosols reaching the sensor directly without contact with the ground, also called the upwelled radiance. Assuming that the first two types of photons are dominant, the spectral radiance at a detector pixel, $L(\lambda)$, can be modeled as,

$$L(\lambda) = kE_s(\lambda) \cos \sigma \tau_d(\lambda) \frac{\rho_t(\lambda)}{\pi} \tau_u(\lambda) + FE_d(\lambda) \frac{\rho_t(\lambda)}{\pi} \tau_u(\lambda), \quad (1)$$

where k is the direct illumination factor and is equal to 0 for targets under shadow and 1 for targets exposed to direct sunlight; $E_s(\lambda)$ is the sun spectral irradiance at a zenith angle of σ , the angle between the surface normal and the sunbeam; $\tau_d(\lambda)$ is the spectral transmission through the atmosphere along the sun-target path, assumed locally spatial-homogeneous; $\rho_t(\lambda)$ is the Lambertian bi-directional reflectance distribution function (BRDF); $\tau_u(\lambda)$ is the spectral transmission along the target-sensor path; F is the sky-view factor or the percent of visible hemisphere sky at the target location; and $E_d(\lambda)$ is the spectral irradiance from the sky.

Letting

$$\beta(\lambda) = E_d(\lambda) \frac{\rho_t(\lambda)}{\pi} \tau_u(\lambda), \quad D(\lambda) = \frac{E_s(\lambda)}{E_d(\lambda)} \tau_d(\lambda),$$

we can rewrite (1) as

$$L(\lambda) = (kD(\lambda) \cos \sigma + F)\beta(\lambda). \quad (2)$$

Under this representation, $\beta(\lambda)$ encapsulates the material reflectance, while $D(\lambda)$ encapsulates the sun, sky and atmospheric parameters. Moreover, in a small local neighborhood, $D(\lambda)$ can be assumed spatially homogeneous and material-independent.

2.2. Calculation of Material Reflectance

Now let us consider two pixels in the detector capturing spectral information of two areas in the scene belonging to the same material, but one in shade and the other directly exposed to the sun. Using (2), for the pixel corresponding to the area exposed to direct sunlight, the observed spectral radiance is,

$$L_1(\lambda) = (D(\lambda) \cos \sigma + F_1)\beta(\lambda). \quad (3)$$

Similarly, for the pixel corresponding to the area under shadow, the observed spectral radiance is,

$$L_2(\lambda) = F_2\beta(\lambda). \quad (4)$$

HSI data provides values for L_1 and L_2 and LiDAR data can be used to estimate the sky view factors F_1 and F_2 , the surface normal, and hence the zenith angle σ . With these values, we can solve (3) for $D(\lambda)$, i.e.

$$D(\lambda) = \sec \sigma \left(\frac{L_1(\lambda)}{L_2(\lambda)} F_2 - F_1 \right). \quad (5)$$

Assuming $D(\lambda)$ is locally homogeneous, we can use it to solve for $\beta(\lambda)$ for other pixels in the neighborhood of the pixel corresponding to the area under shadow, i.e.,

$$\beta(\lambda) = \frac{L(\lambda)}{kD(\lambda) + F}. \quad (6)$$

Because $\beta(\lambda)$ is only different from the material reflectance, $\rho_t(\lambda)$, by a couple factors that are homogeneous in a local neighborhood, we propose the idea of classifying materials using $\beta(\lambda)$. Though some well-known characteristic features of materials may be lost, the resulting spectral vectors may be less sensitive to changes in illumination and simplify subsequent detection, classification, and identification tasks [1].

2.3. Selecting Material Data

Manually selecting two pixels corresponding to the same material, one under shadow and the other exposed, can be tedious and error prone. Here, we offer several basic criteria to help identifying such pixels.

1. *Similar radiance profile across bands.* The spectral vectors of two pixels of the same material look similar in shape across the spectral bands, i.e. $\frac{s_1^T s_2}{\|s_1\|_2 \|s_2\|_2} \approx 1$, where s_1, s_2 are two spectral signatures.

2. *Similar heights.* Sometimes pixels corresponding to tree foliage have similar spectral responses as neighboring grass pixels, but they often appear at different heights in LiDAR data. The availability of LiDAR data is very useful in this regard.
3. *Similar and not-too-small sky-view factors.* Neighboring pixels tend to have similar sky-view factors, since they are spatially close. However, as shown in (6), small sky-view factors can lead to unreasonably large $\beta(\lambda)$ so the value of F must be considered carefully.

In practice, these criteria should be combined with expert knowledge or other available information to select appropriate pixel data to calculate $D(\lambda)$ and $\beta(\lambda)$.

2.4. Sky-View Factor from LiDAR Data

We take a similar approach as [8]. For each LiDAR point $p = (x_0, y_0, z_0)$, we scan its neighbors within a given window size, δ , to compute their Cartesian coordinate differences, i.e.,

$$dx_i = x_i - x_0, dy_i = y_i - y_0, dz_i = z_i - z_0, \quad (7)$$

where $|dx_i| \leq \delta, |dy_i| \leq \delta$, and $dz_i \geq 0$ and $i = 1, \dots, n$ is the number of neighbors of p . If we can assume each LiDAR point (x_i, y_i, z_i) represents a horizontal square surface $d \times d$, where d is the ground sampling distance (GSD), then we know the vectors of four corner points to (x_0, y_0, z_0) , denoted as a_i, b_i, c_i , and d_i . Now we have two tetrahedrons formed by vectors (a_i, b_i, c_i) and by vectors (a_i, c_i, d_i) . We can compute the solid angles of each tetrahedron, $\Omega(a_i, b_i, c_i)$, and $\Omega(a_i, c_i, d_i)$, and add them to obtain the solid angles of the square surface. Summing all the solid angles of square surfaces gives the portion of the hemisphere covered by neighboring LiDAR points, and hence the sky-view factor, i.e.

$$F = 1 - \frac{1}{2\pi} \sum_{i=1}^n [\Omega(a_i, b_i, c_i) + \Omega(a_i, c_i, d_i)]. \quad (8)$$

2.5. Estimating Area of Shadow from LiDAR Data

For each LiDAR point $p = (x_0, y_0, z_0)$, if there is a neighboring point, (x_i, y_i, z_i) , that falls in the line between p and the sun, then we assume there is shadow at location (x_0, y_0) . This can be formulated as, $\frac{\Delta p_i^T r_s}{\|\Delta p_i\|_2 \|r_s\|_2} \approx 1$, where $\Delta p_i = (dx_i, dy_i, dz_i)$ and r_s is the sunbeam vector, which is available by knowing the exact time and day of the data collection.

3. EXPERIMENTS

To test our radiance based approach, we employed HSI and LiDAR datasets that were simultaneously acquired by sensors on the same aircraft, taken at approximately 11:30 am on November 8th, 2010, at Gulfport, Mississippi [9]. The

ground sampling distance is 1 meter. The original HSI dataset has 72 bands ranging from $.4\mu m$ to $1.0\mu m$. After removing noisy bands, we use 58 bands on a 56×74 scene, and the co-registered LiDAR data is simply a 320×360 height-profile matrix.

Figure 2(a) shows the RGB image of the scene, at the center of which is a paved round-about, partly shaded by a large tree, and other objects such as building roofs and parking lots. These areas are marked with text in Figure 2(a). First we applied a texture-based total variation classification method to the corresponding observed radiance data, resulting in the map shown in Figure 2(b), where the dark blue areas are shadows. We then applied the radiance model to remove the atmospheric parameter $D(\lambda)$ from the scene, using pixels from the round-about, parking lot, and building roof for this process. After this correction, the segmentation map in Figure 2(c) shows the shadow areas removed from the scene, and shows a clear continuation of the round-about in the tree shadow, and the pavement even continues onto the parking lot to the left. In this particular classification, we have grouped green areas together (trees and grass) regardless of whether they are under shade. This shows that the correction method is not limited to one particular material. We can also see a smaller paved circle at the center of the round-about partly shaded by the tree, which is then confirmed by the street view.

4. DISCUSSIONS AND CONCLUSIONS

In this paper we have proposed a simple radiance correction method to directly compare spectral signatures of pixels corresponding to areas with and without direct sun exposure. Such comparisons arise in the classification of materials or targets hidden under shadows. The proposed method avoids using the atmosphere correction and specialized packages, while quickly identifying objects of interest or targets for further analysis. There are several limitations of the method.

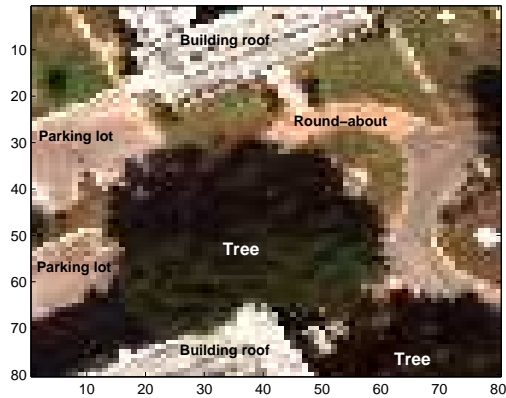
1. *Locality.* In a small neighborhood we assume spatial homogeneity for the sun irradiance, the diffused sky-light, the sun-target path, and the target-sensor path. Hence to apply this method, the scene in consideration can not be too large.
2. *No adjacency or background effect.* Since we have ignored the adjacency and upwelling radiance effects in $L(\lambda)$, the method can not be applied to areas such as the foot of a building, where photons bouncing off the building's walls would significantly contribute to the observed radiance, or small sky-view factor areas such as narrow space between trees.
3. *Expert knowledge in choosing the pixel pairs.* Finding two similar pixels of the same material with one in shade and the other exposed could be difficult, and some expert knowledge or additional information can be helpful, after applying the provided criteria.

5. ACKNOWLEDGMENT

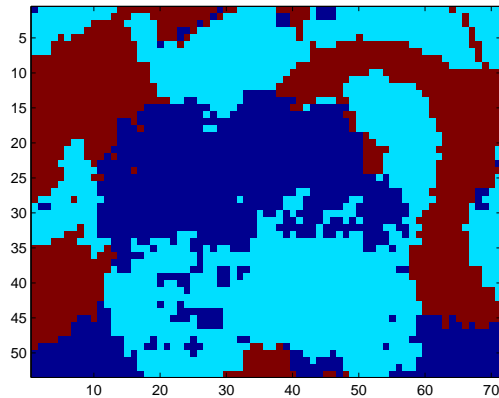
The domestic overhead imagery collection was authorized under NGA PUM 12-022 with permission obtained by a Letter of Consent from the University of Southern Mississippi to the University of Florida.

6. REFERENCES

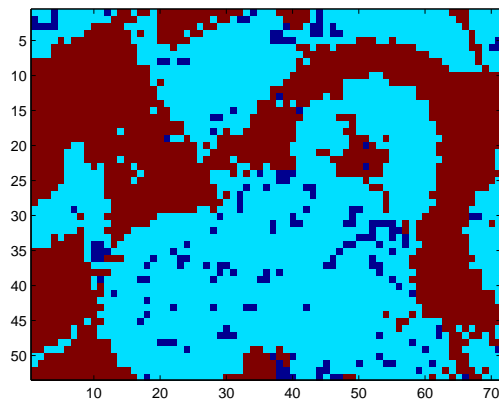
- [1] M. T. Eismann, *Hyperspectral Remote Sensing*, SPIE Press, 2012.
- [2] M.T. Eismann, "Strategies for hyperspectral target detection in complex background environments," in *Aerospace Conference, 2006 IEEE*. IEEE, 2006, pp. 10–pp.
- [3] A.P. Cracknell and L. Hayes, *Introduction to remote sensing*, CRC press, 1991.
- [4] M. Dalponte, L. Bruzzone, and D. Gianelle, "Fusion of hyperspectral and lidar remote sensing data for classification of complex forest areas," *Geoscience and Remote Sensing, IEEE Transactions on*, vol. 46, no. 5, pp. 1416–1427, 2008.
- [5] T.L. Erdody and L.M. Moskal, "Fusion of lidar and imagery for estimating forest canopy fuels," *Remote Sensing of Environment*, vol. 114, no. 4, pp. 725–737, 2010.
- [6] M. Shimoni, G. Tolt, C. Perneel, and J. Ahlberg, "Detection of vehicles in shadow areas," in *Hyperspectral Image and Signal Processing: Evolution in Remote Sensing (WHISPERS), 2011 3rd Workshop on*. IEEE, 2011, pp. 1–4.
- [7] E.J. Ientilucci, "Leveraging lidar data to aid in hyperspectral image target detection in the radiance domain," in *Proceedings of SPIE*, 2012, vol. 8390, p. 839007.
- [8] A. Berk, G.P. Anderson, P.K. Acharya, L.S. Bernstein, L. Muratov, J. Lee, M. Fox, S.M. Adler-Golden, J.H. Chetwynd, M.L. Hoke, et al., "Modtran 5: a reformulated atmospheric band model with auxiliary species and practical multiple scattering options: update," in *Proceedings of SPIE*, 2005, vol. 5806, p. 662.
- [9] J.R. Schott, *Remote sensing: the image chain approach*, Oxford University Press, USA, 2007.
- [10] C. Kidd and L. Chapman, "Derivation of sky-view factors from lidar data," *International Journal of Remote Sensing*, vol. 33, no. 11, pp. 3640–3652, 2012.
- [11] P. Gader, A. Zare, R. Close, and G. Tuell, "Co-registered hyperspectral and LiDAR Long Beach, Mississippi data collection," 2010, University of Florida, University of Missouri, and Optech International.



(a) RGB Image.



(b) Radiance segmentation.



(c) Corrected radiance segmentation.

Fig. 2. Scene I: a round-about in front of a building.